Determining Aircraft Moments of Inertia from Flight Test Data

Eugene A. Morelli[1]

NASA Langley Research Center, Hampton, Virginia, 23666

https://doi.org/10.2514/1.G006072

Flight test maneuvers and dynamic modeling techniques were developed for determining aircraft moments of inertia from flight test data. Full nonlinear rigid-body rotational equations of motion were used in the analysis, with aerodynamic moment dependencies modeled by linear expansions in the aircraft states and controls. Aerodynamic parameters were estimated simultaneously with inertia parameters using equation-error modeling applied to flight test data from maneuvers designed specifically for this problem. The approach was demonstrated using a nonlinear F-16 simulation, then applied to a remotely-piloted subscale aircraft flight test. Errors in the aircraft moment of inertia parameters determined from simulated F-16 flight test data were less than 6% compared to the true values in the simulation. Flight test results for the subscale aircraft were within 6% of ground-test values obtained using the same aircraft.

Nomenclature

b	=	wing span, ft
$\bar{c}$	=	wing mean aerodynamic chord, ft
C_l, C_m, C_n	=	nondimensional aerodynamic roll, pitch, and yaw moment coefficients
I_p	=	propulsion system rotational moment of inertia, slug-ft^2

Presented as Paper 2021-1642 at the 2021 AIAA SciTech Forum, Virtual Event, January 11-21, 2021

[1] Research Engineer, Dynamic Systems and Control Branch, AIAA Associate Fellow

I_x, I_y, I_z, I_{xz} = moments of inertia, slug-ft^2

L, M, N = aerodynamic roll, pitch, and yaw moments, ft-lbf

m = aircraft mass, slug

p, q, r = body-axis roll, pitch, and yaw angular rates, rad/s or deg/s

$\dot{p}, \dot{q}, \dot{r}$ = body-axis roll, pitch, and yaw angular accelerations, rad/s^2 or deg/s^2

$\bar{q}$ = dynamic pressure, lbf/ft^2

rms = root mean square

S = wing reference area, ft^2

T = maneuver length, s

V = true airspeed, ft/s

α = angle of attack, rad or deg

β = sideslip angle, rad or deg

$\delta_s, \delta_e, \delta_a, \delta_r$ = stabilator, elevator, aileron, and rudder deflections, rad or deg

Ω_p = propulsion system rotational speed, rad/s

subscripts

cg = center of gravity

o = reference value or bias term

l, r = left, right

I. Introduction

STABILITY and control flight testing for fixed-wing aircraft is typically focused on modeling nondimensional aerodynamic forces and moments as a function of explanatory variables such as angle of attack, sideslip angle, body-axis angular rates, and control surface deflections. The nondimensionalization involves dynamic pressure, which is easily measured in flight, and mass/inertia properties [1]. Mass/inertia properties can be obtained from ground tests [2-17] or by carefully constructing a computer-aided design (CAD) model of the aircraft [18-21], along with careful accounting for fuel weight and loading. Determining aircraft mass on the ground is simple, but ground

testing for determining moments of inertia is both costly and time-consuming, and can sometimes result in damage to the aircraft. In addition, any substantial change to the aircraft configuration incurs changes in the inertia properties, which requires either an adjustment to previous ground test results or a repeat of the ground tests. Using a CAD model requires detailed knowledge of the mass and location of all aircraft components, which also must be carefully updated for any aircraft configuration changes.

Previous work has addressed the problem of determining inertia properties from flight data for quadrotors [22-23] and spacecraft [24-27], assuming that the applied moments are known. For fixed-wing aircraft flying in the atmosphere, the problem is more complicated, because the applied moments from aerodynamics cannot be treated as known.

In this work, novel flight test maneuvers and dynamic modeling techniques were developed to determine the moments of inertia for symmetric fixed-wing aircraft from flight test data alone. The approach requires an instrumented aircraft capable of controlled flight test maneuvers with high angular rates. Unmanned rapid-prototype aircraft or subscale research aircraft can satisfy these requirements. For other flight testing, the method might be used to validate or corroborate ground test results, or to determine the changes in moments of inertia associated with aircraft configuration changes.

The general idea is to fly a maneuver at low nominal angle of attack with small excursions in angle of attack and sideslip angle induced by low-amplitude perturbations of the control surfaces, while simultaneously invoking high-amplitude body-axis angular rates. This keeps the aircraft aerodynamic dependencies approximately linear, while enhancing the nonlinear terms in the rotational dynamic equations of motion that involve the aircraft moments of inertia. Because the terms associated with the aircraft moments of inertia are nonlinear in the angular rates and different from aerodynamic dependencies for small perturbations in angle of attack and sideslip angle at low nominal angles of attack, both the linear aerodynamic parameters and the moment of inertia parameters can be estimated accurately and simultaneously using equation-error parameter estimation applied to the flight data.

The next section explains the method, including the equations, modeling computations, and the flight test maneuver design. In Section III, the F-16 nonlinear simulation and the E1 subscale aircraft are described. Section IV demonstrates an application of the method using simulated flight data from the F-16 nonlinear simulation with realistic measurement noise and known moments of inertia. In Section V, the method is applied to flight test data from the E1 subscale aircraft flown by a pilot on the ground using conventional radio control and automated

excitation inputs applied to the control surfaces. Aircraft moments of inertia from ground testing for this aircraft were used for comparison with the flight test results. Section VI provides a discussion of the methods and results and Section VII contains conclusions.

All of the flight test maneuver design, flight simulation, data analysis, and modeling tasks for this work were done using a software toolbox written in MATLAB® called System IDentification Programs for AirCraft (SIDPAC) [1,28]. SIDPAC was developed at NASA Langley and has been applied successfully to a wide variety of flight test and wind tunnel experiments. SIDPAC has been used at more than 100 organizations worldwide to solve aircraft system identification problems [29].

II. Method

Determining aircraft moments of inertia from flight test data involves appropriate equations of motion, modeling assumptions and techniques for estimating the unknown model parameters, along with specific flight test maneuvers to generate suitable flight data.

A. Equations of Motion

The nonlinear equations of motion for the rigid-body rotational dynamics of a symmetric fixed-wing aircraft with thrust acting along the *x* body axis are [1]:

$$I_x\dot{p} - I_{xz}\dot{r} = L + \left(I_y - I_z\right)qr + I_{xz}pq \tag{1}$$

$$I_y\dot{q} = M + \left(I_z - I_x\right)pr + I_{xz}\left(r^2 - p^2\right) + I_p\Omega_p r \tag{2}$$

$$I_z\dot{r} - I_{xz}\dot{p} = N + \left(I_x - I_y\right)pq - I_{xz}qr - I_p\Omega_p q \tag{3}$$

For a conventional airplane, if the flight test maneuver is conducted so that the aerodynamic dependencies can be modeled using linear expansions in the aircraft states and controls,

$$L = \bar{q}Sb\left(C_{l_o} + C_{l_\beta}\beta + C_{l_p}\frac{pb}{2V} + C_{l_r}\frac{rb}{2V} + C_{l_{\delta_a}}\delta_a + C_{l_{\delta_r}}\delta_r\right) \tag{4}$$

$$M = \bar{q}S\bar{c}\left(C_{m_o} + C_{m_\alpha}\alpha + C_{m_q}\frac{q\bar{c}}{2V} + C_{m_{\delta_e}}\delta_e\right) \tag{5}$$

$$N = \bar{q}Sb\left(C_{n_o} + C_{n_\beta}\beta + C_{n_p}\frac{pb}{2V} + C_{n_r}\frac{rb}{2V} + C_{n_{\delta_a}}\delta_a + C_{n_{\delta_r}}\delta_r\right) \tag{6}$$

Combining Eqs. (1)-(6) gives the rotational equations of motion with nonlinear dynamics and linear aerodynamics,

$$I_x\dot{p} - I_{xz}\dot{r} = \bar{q}Sb\left(C_{l_o} + C_{l_\beta}\beta + C_{l_p}\frac{pb}{2V} + C_{l_r}\frac{rb}{2V} + C_{l_{\delta_a}}\delta_a + C_{l_{\delta_r}}\delta_r \right) + \left(I_y - I_z\right)qr + I_{xz}pq \tag{7}$$

$$I_y\dot{q} = \bar{q}S\bar{c}\left(C_{m_o} + C_{m_\alpha}\alpha + C_{m_q}\frac{q\bar{c}}{2V} + C_{m_{\delta_e}}\delta_e \right) + \left(I_z - I_x\right)pr + I_{xz}\left(r^2 - p^2\right) + I_p\Omega_p r \tag{8}$$

$$I_z\dot{r} - I_{xz}\dot{p} = \bar{q}Sb\left(C_{n_o} + C_{n_\beta}\beta + C_{n_p}\frac{pb}{2V} + C_{n_r}\frac{rb}{2V} + C_{n_{\delta_a}}\delta_a + C_{n_{\delta_r}}\delta_r \right) + \left(I_x - I_y\right)pq - I_{xz}qr - I_p\Omega_p q \tag{9}$$

Rearranging,

$$\dot{p} = \frac{\bar{q}Sb}{I_x}\left(C_{l_o} + C_{l_\beta}\beta + C_{l_p}\frac{pb}{2V} + C_{l_r}\frac{rb}{2V} + C_{l_{\delta_a}}\delta_a + C_{l_{\delta_r}}\delta_r \right) + c_1 qr + c_2\left(\dot{r} + pq\right) \tag{10}$$

$$\dot{q} = \frac{\bar{q}S\bar{c}}{I_y}\left(C_{m_o} + C_{m_\alpha}\alpha + C_{m_q}\frac{q\bar{c}}{2V} + C_{m_{\delta_e}}\delta_e \right) + c_3\, pr + c_4\left(r^2 - p^2\right) + \frac{I_p}{I_y}\Omega_p\, r \tag{11}$$

$$\dot{r} = \frac{\bar{q}Sb}{I_z}\left(C_{n_o} + C_{n_\beta}\beta + C_{n_p}\frac{pb}{2V} + C_{n_r}\frac{rb}{2V} + C_{n_{\delta_a}}\delta_a + C_{n_{\delta_r}}\delta_r \right) + c_5\, pq + c_6\left(\dot{p} - qr\right) - \frac{I_p}{I_z}\Omega_p\, q \tag{12}$$

where

$$c_1 = \left(I_y - I_z\right)/I_x \qquad c_2 = I_{xz}/I_x \tag{13a}$$

$$c_3 = \left(I_z - I_x\right)/I_y \qquad c_4 = I_{xz}/I_y \tag{13b}$$

$$c_5 = \left(I_x - I_y\right)/I_z \qquad c_6 = I_{xz}/I_z \tag{13c}$$

The aerodynamic bias terms C_{l_o}, C_{m_o}, C_{n_o} must be retained in Eqs. (10)-(12), because the nonlinear equations of motion are being used. Propulsion system rotational inertia I_p can be determined from simple ground tests or from manufacturer data, and the propulsion system rotational speed Ω_p can be measured, so that the gyroscopic terms involving the propulsion system angular momentum $I_p\Omega_p$ can be treated as known. The propulsion terms can also be made small by executing the flight test maneuver at idle power to reduce Ω_p. For most fixed-wing aircraft, the ratios I_p/I_y and I_p/I_z will be small, so that the propulsion terms can be negligible compared to the other terms in the equation. Another approach is to estimate the propulsion system inertia I_p as an additional unknown parameter,

which can be done when the propulsion system rotational speed Ω_p is measured and varied substantially during the maneuver.

There are six inertia constants in Eq. (13), but only four inertia tensor elements for a symmetric aircraft, namely $I_x, I_y, I_z,$ and I_{xz} . Consequently, only four of the inertia constants in Eq. (13) need to be estimated in order to obtain values for I_x, I_y, I_z, and I_{xz} .

B. Modeling

If the nominal angle of attack during the flight test maneuver is low but the angular rates are high, then Eqs. (10)-(12) can be used to estimate both the aerodynamic parameters and the inertia parameters. Note that the nonlinear angular rate and angular acceleration terms associated with the inertia parameters are typically not necessary for aerodynamic modeling at low nominal angles of attack, so that these terms can be associated solely with the inertia effects. All of the inertia parameters in the pitch equation (11) and the yaw equation (12) are multiplied by the roll rate p or the roll acceleration $\dot{p}$, and the four inertia parameters in Eqs. (11)-(12) involve all four of the inertia tensor elements. In contrast, the roll equation has the nonlinear term qr, which is difficult to make large while maintaining a low nominal angle of attack. Furthermore, the rolling motion of the aircraft needed for sufficient amplitude of the inertial terms in the pitch and yaw equations leads to large aerodynamic terms in the roll equation. In that case, aerodynamic terms dominate the inertia terms in the roll equation, which makes the inertia terms in the roll equation difficult to determine accurately. A good approach is to use flight test maneuvers with large-amplitude changes in roll rate, then analyze the data using only the pitch and yaw moment equations.

Because the airspeed V and the dynamic pressure $\bar{q}$ change significantly for most high-amplitude maneuvers, those dependencies must be retained in the aerodynamic modeling. Equations (10)-(12) can be written as

$$\dot{p} = \bar{q} L_o + \bar{q} L_\beta \beta + \bar{q} L_p \frac{p}{V} + \bar{q} L_r \frac{r}{V} + \bar{q} L_{\delta_a} \delta_a + \bar{q} L_{\delta_r} \delta_r + c_1 qr + c_2 \left(\dot{r} + pq \right) \tag{14}$$

$$\dot{q} = \bar{q} M_o + \bar{q} M_\alpha \alpha + \bar{q} M_q \frac{q}{V} + \bar{q} M_{\delta_e} \delta_e + c_3 pr + c_4 \left(r^2 - p^2 \right) + \frac{I_p}{I_y} \Omega_p r \tag{15}$$

$$\dot{r} = \bar{q} N_o + \bar{q} N_\beta \beta + \bar{q} N_p \frac{p}{V} + \bar{q} N_r \frac{r}{V} + \bar{q} N_{\delta_a} \delta_a + \bar{q} N_{\delta_r} \delta_r + c_5 pq + c_6 \left(\dot{p} - qr \right) - \frac{I_p}{I_z} \Omega_p q \tag{16}$$

where

$$L_o = \frac{Sb}{I_x} C_{l_o} \quad L_\beta = \frac{Sb}{I_x} C_{l_\beta} \quad L_p = \frac{Sb^2}{2I_x} C_{l_p} \quad L_r = \frac{Sb^2}{2I_x} C_{l_r} \quad L_{\delta_a} = \frac{Sb}{I_x} C_{l_{\delta_a}} \quad L_{\delta_r} = \frac{Sb}{I_x} C_{l_{\delta_r}} \tag{17a}$$

$$M_o = \frac{S\bar{c}}{I_y} C_{m_o} \quad M_\alpha = \frac{S\bar{c}}{I_y} C_{m_\alpha} \quad M_q = \frac{S\bar{c}^2}{2I_y} C_{m_q} \quad M_{\delta_e} = \frac{S\bar{c}}{I_y} C_{m_{\delta_e}} \tag{17b}$$

$$N_o = \frac{Sb}{I_z} C_{n_o} \quad N_\beta = \frac{Sb}{I_z} C_{n_\beta} \quad N_p = \frac{Sb^2}{2I_z} C_{n_p} \quad N_r = \frac{Sb^2}{2I_z} C_{n_r} \quad N_{\delta_a} = \frac{Sb}{I_z} C_{n_{\delta_a}} \quad N_{\delta_r} = \frac{Sb}{I_z} C_{n_{\delta_r}} \tag{17c}$$

Although the unknown parameters specified in Eq. (17) involve both aerodynamics and inertia, these quantities can be considered constant for a flight test maneuver executed at low nominal angle of attack. The definitions in Eq. (17) are not the usual definitions of dimensional derivatives, because dynamic pressure and airspeed are specified separately in Eqs. (14)-(16). Estimates of the unknown parameters defined in Eq. (17) will not be useful directly for aerodynamic modeling, but rather are used as a means toward the goal of estimating the inertia parameters. The inertia parameters are determined from a flight test maneuver designed to make the nonlinear inertia terms significant. The resulting inertia tensor element values can then be used to compute nondimensional aerodynamic model parameters using Eq. (17), or in separate analyses of standard small-amplitude maneuvers, where the nonlinear inertial terms are assumed negligible because of low angular rates.

Equations (14)-(16) are coupled nonlinear equations with unknown parameters characterizing the linear aerodynamic dependencies and the moments of inertia. Using only Eqs. (15) and (16) for the modeling, and assuming that the flight test maneuver is executed at idle power to make the propulsion system gyroscopic terms negligible, the vector of unknown parameters $\boldsymbol{\theta}$ is

$$\boldsymbol{\theta} \equiv \begin{bmatrix} M_o & M_\alpha & M_q & M_{\delta_e} & c_3 & c_4 & N_o & N_\beta & N_p & N_r & N_{\delta_a} & N_{\delta_r} & c_5 & c_6 \end{bmatrix}^T \tag{18}$$

If the roll equation (14) is omitted from the analysis, then the flight data for roll rate p and roll acceleration $\dot{p}$ can be substituted as measured values in Eqs. (15) and (16). This helps the modeling by reducing the number of unknown parameters without compromising the goal of accurately estimating at least four inertia parameters, which are $c_3, c_4, c_5,$ and c_6 in Eqs. (15) and (16).

The resulting modeling problem can be solved using equation-error parameter estimation with nonlinear model terms in either the time domain [1] or the frequency domain [1,30]. Because the model structure for the problem is

fixed, real-time parameter estimation methods [1,30] can be used as well. The problem can also be formulated as a nonlinear output-error parameter estimation problem in the time domain, which can be solved using standard optimization routines [1,31].

In this work, equation-error in the time domain was used with smoothed explanatory variable data to obtain accurate and unbiased parameter estimates [1,32]. This approach allows easy incorporation of data from multiple maneuvers and the capability to selectively include or exclude data points that are not necessarily contiguous in time. These features are helpful for improving relevant data information content by including data from multiple maneuvers at low nominal angles of attack where a linear aerodynamic model is valid.

The equation-error approach also allows modeling using one equation at a time. For example, the equation-error parameter estimation problem for the pitching moment equation (15) with N data points is

$$\boldsymbol{z} = \boldsymbol{X}\boldsymbol{\theta} + \boldsymbol{\varepsilon} \tag{19}$$

where

$\boldsymbol{z} = \begin{bmatrix} \dot{q}(1) & \dot{q}(2) & \dots & \dot{q}(N) \end{bmatrix}^T$ = vector of output measurements

$$\boldsymbol{X} = \begin{bmatrix} \bar{q}(1) & \bar{q}(1)\alpha(1) & \bar{q}(1)\dfrac{q(1)}{V(1)} & \bar{q}(1)\delta_e(1) & p(1)r(1) & r^2(1)-p^2(1) \\ \bar{q}(2) & \bar{q}(2)\alpha(2) & \bar{q}(2)\dfrac{q(2)}{V(2)} & \bar{q}(2)\delta_e(2) & p(2)r(2) & r^2(2)-p^2(2) \\ \vdots & \vdots & \vdots & \vdots & \vdots & \vdots \\ \bar{q}(N) & \bar{q}(N)\alpha(N) & \bar{q}(N)\dfrac{q(N)}{V(N)} & \bar{q}(N)\delta_e(N) & p(N)r(N) & r^2(N)-p^2(N) \end{bmatrix} = \text{matrix of modeling function vectors}$$

$\boldsymbol{\theta} \equiv \begin{bmatrix} M_o & M_\alpha & M_q & M_{\delta_e} & c_3 & c_4 \end{bmatrix}^T$ = vector of unknown parameters

$\boldsymbol{\varepsilon} = \begin{bmatrix} \varepsilon(1) & \varepsilon(2) & \dots & \varepsilon(N) \end{bmatrix}^T$ = vector of equation errors

The matrix $\boldsymbol{X}$ is assembled using measured data, with each column representing a modeling function, also called a regressor. The measured output data $\boldsymbol{z}$ is computed as a smoothed numerical derivative of the measured angular rates [1,32]. The best estimate of $\boldsymbol{\theta}$ in a least-squares sense comes from minimizing the sum of squared differences between the measured output $\boldsymbol{z}$ and the model output $\boldsymbol{y} = \boldsymbol{X}\boldsymbol{\theta}$,

$$J(\boldsymbol{\theta}) = \frac{1}{2}(\boldsymbol{z} - \boldsymbol{X}\boldsymbol{\theta})^T(\boldsymbol{z} - \boldsymbol{X}\boldsymbol{\theta}) \tag{20}$$

The least-squares solution for the unknown parameter vector $\boldsymbol{\theta}$ is [1]

$$\hat{\boldsymbol{\theta}} = \left(\boldsymbol{X}^T\boldsymbol{X}\right)^{-1}\boldsymbol{X}^T\boldsymbol{z} \tag{21}$$

and the estimated model output is

$$\hat{\boldsymbol{y}} = \boldsymbol{X}\hat{\boldsymbol{\theta}} \tag{22}$$

The estimated parameter covariance matrix is computed from [1]

$$Cov\left(\hat{\boldsymbol{\theta}}\right) = \hat{\sigma}^2\left(\boldsymbol{X}^T\boldsymbol{X}\right)^{-1} \equiv \left[C_{ij}\right] \qquad i,j = 1,2,\ldots,n_p \tag{23a}$$

$$\hat{\sigma}^2 = \frac{\left(\boldsymbol{z}-\hat{\boldsymbol{y}}\right)^T\left(\boldsymbol{z}-\hat{\boldsymbol{y}}\right)}{\left(N-n_p\right)} \tag{23b}$$

where n_p is the number of unknown parameters, and $n_p = 6$ for this example. Modifications of Eq. (23) are required when the residuals $\left(\boldsymbol{z}-\hat{\boldsymbol{y}}\right)$ are colored [1,32]. The standard errors of the estimated parameters are given by the square root of the diagonal elements of the covariance matrix,

$$s\left(\hat{\theta}_j\right) = \sqrt{C_{jj}} \qquad j = 1,2,\ldots,n_p \tag{24}$$

Equation-error modeling for the yawing moment Eq. (16) is similar. The inertia parameters $c_3, c_4, c_5,$ and c_6 in Eqs. (15) and (16) are linear model parameters in the equation-error formulation, because the parameters appear linearly in the equations. If instead the unknown inertia parameters are changed to the inertia tensor elements $I_x, I_y, I_z,$ and I_{xz} , then these unknown inertia parameters appear nonlinearly in the equations, which requires a nonlinear optimizer for the solution [1]. Either of these approaches can be readily implemented using SIDPAC.

In Eqs. (14)-(16), the aerodynamic parameters are multiplied by terms that are linear in sideslip angle, angle of attack, angular rates, and control surface deflections, whereas the moment of inertia parameters are multiplied by angular accelerations and nonlinear functions of the angular rates. This distinction is the basis for the ability to identify aerodynamic parameters and the moment of inertia parameters simultaneously. However, to do so requires a flight test maneuver for which the aerodynamic dependencies can be considered linear while the angular rates and angular accelerations change significantly. Flight test maneuvers with these characteristics are described next.

C. Flight Test Maneuver Design

The flight test maneuver design has two objectives: 1) achieve large-amplitude angular rates, so that the nonlinear terms associated with the inertia parameters are significant, and 2) excite the aerodynamic explanatory variables in an uncorrelated way at low nominal angle of attack, to enable accurate linear aerodynamic model

parameter estimation. These objectives can be achieved by flying a large-amplitude maneuver with orthogonal optimized multisine excitations active throughout the maneuver.

1. Large-Amplitude Maneuver

Relatively large angular rates can be achieved at low nominal angle of attack by rolling about the velocity vector [33] into descending turns. As discussed earlier, the nonlinear inertia terms in the pitch and yaw equations all involve roll rate or roll acceleration. Velocity-vector rolls into descending turns with approximately constant nominal angle of attack were found to be effective for raising the roll rate and roll acceleration amplitudes with simultaneous pitch and yaw rates, and are reasonable to fly. Following alternating descending turns, a gradual pullup can be used to arrest the aircraft descent and increase the pitch rate. Variations of this sequence or other flight test maneuvers of this kind can also be acceptable, as will be discussed in the application examples.

For linear aerodynamic parameter estimation, uncorrelated excitations of the explanatory variables about the nominal flight condition are required. This excitation was provided by automated orthogonal optimized multisine inputs [1,30,34-37], described next. These perturbation inputs are balanced about zero with minimized amplitude excursions, so that the aircraft maintains its nominal trajectory, but the aerodynamic explanatory variables are excited in an uncorrelated manner, enabling accurate linear aerodynamic parameter estimation. These inputs also excited the angular rates, so that the nonlinear terms associated with the inertia parameters were further enhanced. Automated orthogonal optimized multisine inputs were applied to multiple control surfaces simultaneously throughout the large-amplitude maneuvers. These automated excitation inputs were called Programmed Test Inputs (PTIs) for both the F-16 nonlinear simulation and the E1 flight tests.

2. Orthogonal Optimized Multisine Inputs

The general idea for the small-amplitude excitations (PTIs) is to move the aircraft control surfaces in a manner that decorrelates the explanatory variables, using perturbation inputs with wideband frequency content encompassing the expected modal frequencies of the aircraft dynamic response. The excitations are implemented by summing designed perturbation inputs with the actuator commands from the pilot and/or feedback control system, just before the limiting on actuator command rates and positions. This implementation is important for achieving the required excitation and low correlations in the explanatory variables.

Each designed perturbation input is a sum of sinusoids with unique harmonic frequencies, optimized phase angles, and specified power distribution. The wideband frequency content of the inputs is important because there is naturally some uncertainty as to what the modal frequencies are for the aircraft in flight, and wideband inputs provide robustness to that uncertainty. Multiple inputs are designed to be mutually orthogonal in both the time domain and the frequency domain simultaneously, and are designed for high data information content in all axes, while minimizing excursions from the nominal flight condition. The mutual orthogonality of the inputs allows simultaneous application of multiple inputs, which reduces the required excitation time for a given amount of input energy, or equivalently, increases the amount of input energy injected into the dynamic system over a given time period. The inputs provide continuous, effective, multi-axis excitation as the aircraft flies along a nominal flight trajectory.

Each perturbation input $\boldsymbol{u}_j$ applied to the *j*th control surface is a sum of harmonic sinusoids with unique frequencies and individual phase angles ϕ_{jk},

$$\boldsymbol{u}_j = \sum_{k\in\{1,2,\ldots,M\}} A_{jk} \sin\left(\frac{2\pi k \boldsymbol{t}}{T} + \phi_{jk}\right) \qquad j = 1,2,\ldots,n_i \tag{25}$$

where M is the total number of available harmonic frequencies, T is the time length of the excitation, A_{jk} is the amplitude for the *k*th sinusoidal component, and $\boldsymbol{t}$ is the time vector. Each of the n_i inputs is the sum of selected components from the pool of M harmonic sinusoids with frequencies $\omega_k = 2\pi k/T$, $k = 1,2,\ldots,M$, and $\omega_M = 2\pi M/T$ represents the upper limit of the frequency band for the excitation. The interval $[\omega_1, \omega_M]$ rad/s specifies the frequency range where the aircraft dynamics are expected to lie. Each $\boldsymbol{u}_j$ in Eq. (25) is a PTI applied to an individual control surface.

The mutual orthogonality of the PTIs in the time domain comes from the fact that each input is composed of harmonic sinusoids with the same base period T but unique harmonic frequencies. Orthogonality in the frequency domain comes from using unique frequencies for the component sinusoids in each multisine input. Both orthogonality properties exist simultaneously for all inputs. The mutual orthogonality of the inputs helps the dynamic modeling by completely decorrelating the inputs, which improves the accuracy of control effectiveness estimates and reduces the correlations among the other explanatory variables as well. This property also means that

the PTIs for every control surface can be applied simultaneously, which produces high information content in the data very efficiently.

If the phase angles ϕ_{jk} in Eq. (25) were chosen at random on the interval $(-\pi,\pi]$ rad, then in general, the various harmonic components would add together at some points to produce a multisine input $\boldsymbol{u}_j$ with relatively large amplitude excursions. This is undesirable because such inputs can move the aircraft too far away from the nominal flight condition. To prevent this, the phase angles ϕ_{jk} for each of the selected harmonic components are optimized to minimize the relative peak factor RPF for each input, defined by

$$\mathrm{RPF}\left(\boldsymbol{u}_j\right) = \frac{\max\left(\boldsymbol{u}_j\right) - \min\left(\boldsymbol{u}_j\right)}{2\sqrt{2}\ \mathrm{rms}\left(\boldsymbol{u}_j\right)} \qquad j = 1,2,\ldots,n_i \tag{26}$$

Relative peak factor is a measure of the efficiency of an input for dynamic modeling purposes and is computed as the amplitude range of the input divided by a measure of the input energy. Low values of relative peak factor are desirable for highly efficient and effective modeling because the objective is to excite the aircraft with good input energy over a variety of frequencies while minimizing the input amplitudes in the time domain, to avoid driving the aircraft too far away from the reference condition. For each multisine input $\boldsymbol{u}_j$ in Eq. (25), minimum RPF is achieved by adjusting the phase angles ϕ_{jk} for each individual sinusoidal component of the input. The resulting optimization problem is multi-dimensional and non-convex; however, a simplex algorithm can be applied to find a solution. The orthogonality of the inputs is unaffected by the values chosen for the phase angles ϕ_{jk} [1,34-36].

The integers k specifying the harmonic frequencies for the *j*th input $\boldsymbol{u}_j$ are selected to be unique to that input, but are not necessarily consecutive. A good approach for multiple inputs is to assign the harmonic frequencies to the inputs alternately. This is illustrated in Fig. 1 for the PTI design on the E1 aircraft. There are 4 inputs in this case: left aileron, right aileron, elevator, and rudder. A total of 44 frequencies $(M = 44)$ were used with excitation time period $T = 40$ s over the frequency band [0.05,1.65] Hz. The harmonic frequencies were interleaved among the four inputs to achieve wideband frequency content in each input, provide robustness in the excitation, and enable accurate estimates of individual control surface effectiveness. Because each input has wideband frequency content, the same input design can be applied at various flight conditions, which simplifies the excitation strategy and

reduces flight computer memory requirements. Figure 2 shows time series for the PTIs designed using the frequency content depicted in Fig. 1.

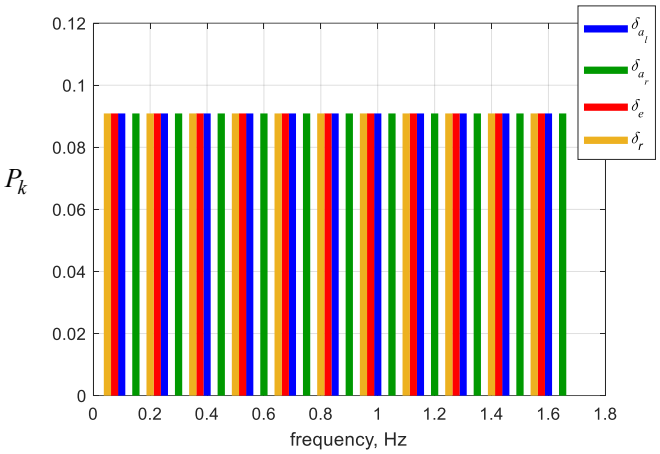

Figure 1. Orthogonal optimized multisine input spectra

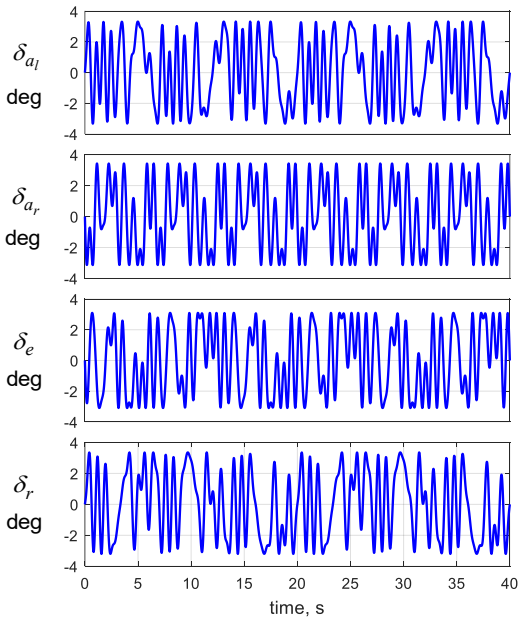

Figure 2. Orthogonal optimized multisine inputs

The sinusoidal components in Eq. (25) can be assigned arbitrary fractions of the total power in the multisine input, to emphasize the excitation at selected frequencies. This is implemented by choosing sinusoidal component amplitudes as

$$A_{jk} = A_j \sqrt{P_{jk}} \tag{27}$$

where A_j is the amplitude of the multisine input $\boldsymbol{u}_j$, and P_{jk} is the power fraction for the kth sinusoidal component of $\boldsymbol{u}_j$. The power fractions for the sinusoidal components in each multisine input must sum to 1,

$$\sum_k P_{jk} = 1 \tag{28}$$

To achieve a uniform power distribution, as shown in Fig. 1, A_{jk} are selected as

$$A_{jk} = \frac{A_j}{\sqrt{M_j}} \tag{29}$$

where M_j is the number of sinusoidal components included in the summation of Eq. (25) for $\boldsymbol{u}_j$, and A_j is the amplitude of the multisine input $\boldsymbol{u}_j$. With uniform power distribution, selection of the A_{jk} reduces to selecting a

single value for the input amplitude A_j. Each input $\boldsymbol{u}_j$ can have arbitrary amplitude A_j, subject to practical flight test and modeling constraints. The power spectra shown in Fig. 1 are power fractions (P_{jk}), so that the individual control surface amplitudes (3 deg for all control surfaces, see Fig. 2) are excluded. SIDPAC program mkmsswp.m was used to design the orthogonal optimized multisine inputs (PTIs) used in this work.

The PTI design shown in Figs. 1 and 2 was used for the E1 flight tests. Because the PTIs are sums of harmonic sinusoids with a common base period *T*, they are periodic for the excitation period *T*, so that the PTIs can be applied repeatedly without any discontinuities in magnitude or slope. The PTI design has minimum RPF and various frequencies and phase angles, which keeps the aircraft response close to the nominal flight trajectory and produces dynamic responses similar to flight in light-to-moderate turbulence. The aircraft response also stays near the nominal flight trajectory because each perturbation input is a sum of harmonic sinusoids, which are all balanced about zero amplitude (equal area above and below zero). The result is rich, dynamic, multi-axis response about the nominal flight trajectory. In practice, pilot inputs and/or automated guidance and control act to spoil the orthogonality (zero pairwise correlations) of the PTI design. However, good modeling results require only low correlations, not zero correlations, so that the slightly correlated inputs that result from applying orthogonal PTIs with pilot inputs and/or automated guidance and control active still work very well in practice.

For flight test situations where an onboard automated excitation system is not available to implement orthogonal optimized multisine inputs, previous flight tests have demonstrated that a test pilot can implement effective multi-axis perturbation inputs with low correlations during large-amplitude maneuvering [38].

III. Aircraft

A. F-16 Nonlinear Simulation

The F-16 is a single-seat, multirole fighter with a blended wing-body and a cropped delta wing planform with leading-edge sweep of 40 deg. Thrust is provided by one General Electric F110-GE-100 or Pratt & Whitney F100-PW-220 afterburning turbofan engine mounted in the rear fuselage. Figure 3 is a photograph of the F-16 in flight. Aircraft geometry and nominal mass/inertia properties are given in Table 1.

The F-16 nonlinear simulation has controls for throttle δ_{th}, stabilator δ_s, aileron δ_a, and rudder δ_r. Speed brake and flaps were assumed fixed at zero deflection.

Figure 3. **F-16 aircraft**
Credit : NASA Langley Research Center

Table 1. **Aircraft geometry and mass/inertia properties**

Property	F-16	E1
$\bar{c}$, ft	11.32	1.97
b , ft	30	10.17
S , ft^2	300	19.26
x_o , ft	$0.35\,\bar{c}$	3.012
y_o , ft	0	0
z_o , ft	0	0
x_{cg} , ft	$0.25\,\bar{c}$	3.027
y_{cg} , ft	0	0.028
z_{cg} , ft	0	−0.248
m , slug	637	1.910
I_x , slug-ft^2	9,496	2.964
I_y , slug-ft^2	55,814	8.776
I_z , slug-ft^2	63,100	11.716
I_{xz} , slug-ft^2	982	0.750

Nondimensional nonlinear aerodynamic force and moment coefficient data were derived from a low-speed static wind-tunnel test and a dynamic forced oscillation wind-tunnel test, both conducted using a 16% scale model of the F-16. The aerodynamic database applies to the F-16 flown out of ground effect, with landing gear retracted and no external stores, over a wide range of angle of attack and sideslip angle.

The F-16 nonlinear simulation was programmed completely in MATLAB®. Full nonlinear equations of motion, including turbine engine gyroscopic effects, were used. Complete details on the F-16 nonlinear simulation can be found in Ref. [1], Appendix D.

B. E1 Aircraft

A subscale aircraft designated E1 was used for flight testing. The E1 aircraft is a commercially available 40% scale Extra 330 SC remotely piloted fixed-wing airplane, shown in Fig. 4. E1 is powered by an electric motor driving a fixed-pitch tractor propeller. Control surfaces are conventional ailerons and trailing-edge flaps on the wings, along with a conventional rudder and split elevator. Aircraft geometry and mass/inertia properties are given in Table 1. More information on the E1 aircraft, flight test instrumentation, and flight test operations can be found in Refs. [39,40].

The flight computer on the E1 aircraft has the capability to inject automated control surface perturbations, called Programmed Test Inputs (PTIs), to excite the aircraft dynamic response and decorrelate the aircraft states and controls, thereby generating flight data with high information content for dynamic modeling. Unique PTIs were applied to each control surface simultaneously, by summing the PTIs with commands from the pilot, just before the limiting on control surface actuator command rates and positions. Flight data used in this work were collected at 50 Hz with the PTIs active and a radio-control pilot on the ground flying the aircraft through large-amplitude maneuvers.

***Figure 4*. E1 aircraft**
Credit : NASA Langley Research Center

IV. F-16 Nonlinear Simulation Example

The F-16 nonlinear simulation described earlier was used to demonstrate the method for estimating moments of inertia from flight test data. The flight test maneuver was composed of piloted alternating velocity-vector roll entries into descending turns followed by a gradual pullup to arrest the descent while maintaining low nominal angle of attack, with automated orthogonal optimized multisine input excitations (PTIs) active throughout the maneuver. The maneuver was flown at idle power, which made the gyroscopic terms from the propulsion system angular momentum negligible. Figure 5 shows the aircraft control surface deflections and response data. Gaussian white noise was added to the simulation outputs, with noise magnitudes chosen to achieve signal-to-noise ratio of approximately 20 for each aircraft response. Note that the angle of attack and sideslip angle varied over a relatively small range near their nominal values while the angular rates exhibited large amplitudes, particularly the roll rate. This was done to keep the aerodynamic dependencies approximately linear while making the nonlinear terms associated with the inertia parameters too large to ignore in the modeling.

Equation-error parameter estimation in the time domain was applied to the simulated flight test data, as described earlier, using SIDPAC program lesq.m. Angular accelerations were computed by applying global Fourier smoothing with SIDPAC program smoo.m, followed by numerical differentiation using SIDPAC program deriv.m. Global Fourier smoothing was also applied to the explanatory variable time series data to avoid parameter estimate bias errors that occur when the modeling functions are noisy [1,32]. The aerodynamic and inertia parameters were

estimated in the pitch moment equation (15) and the yaw moment equation (16), analyzed individually. A comparison of the inertia parameter estimates from simulated flight test data with the known inertia parameters for the F-16 nonlinear simulation is shown in Table 2. The inertia parameters estimated from simulated flight test data are within 6% of the true values, with the mean absolute error less than 4%. Standard errors given in Table 2 were corrected for colored residuals using SIDPAC program r_colores.m [1]. All true values of the inertia parameters were within ±2 standard errors of the values estimated from simulated flight test data, indicating that the estimates were in statistical agreement with the true values. This demonstrates the effectiveness of the approach using realistic simulated flight test data from a large-amplitude maneuver flown by a pilot with PTIs active.

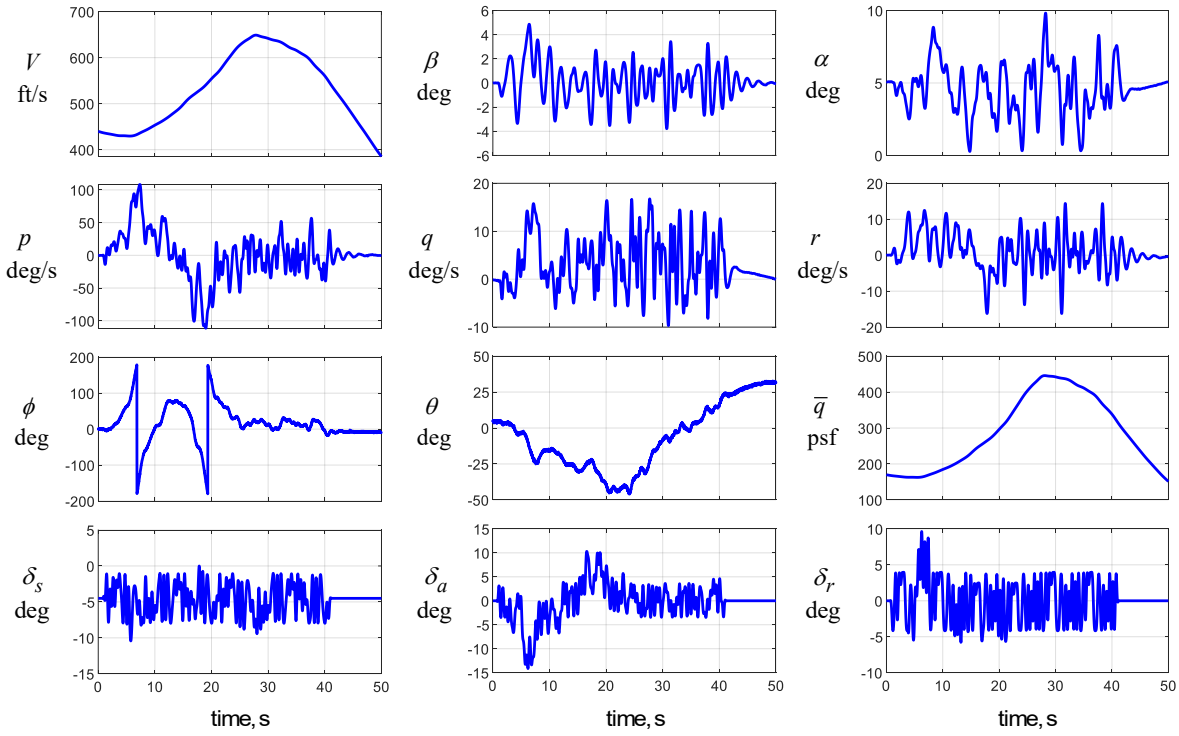

Figure 5. **F-16 large-amplitude maneuver data with PTIs active**

***Table 2*. F-16 Inertia Parameters**

Parameter	True	Estimate ± Standard Error	Percent Error
c_3	0.9604	0.9643 ± 0.0234	0.40
c_4	0.0176	0.0166 ± 0.0019	–5.68
c_5	–0.7340	–0.7517 ± 0.0189	–2.41
c_6	0.0156	0.0147 ± 0.0011	–5.25

Figure 6 shows that the model fits to the simulated flight data for angular acceleration in pitch and yaw were accurate, with coefficients of determination R^2 equal to 99.9% and 99.8%, respectively. The R^2 metric quantifies the model fit to the variation about the mean value for the measured outputs, which are the pitch and yaw angular acceleration data in Fig. 6. More information on the R^2 metric can be found in Ref. [1].

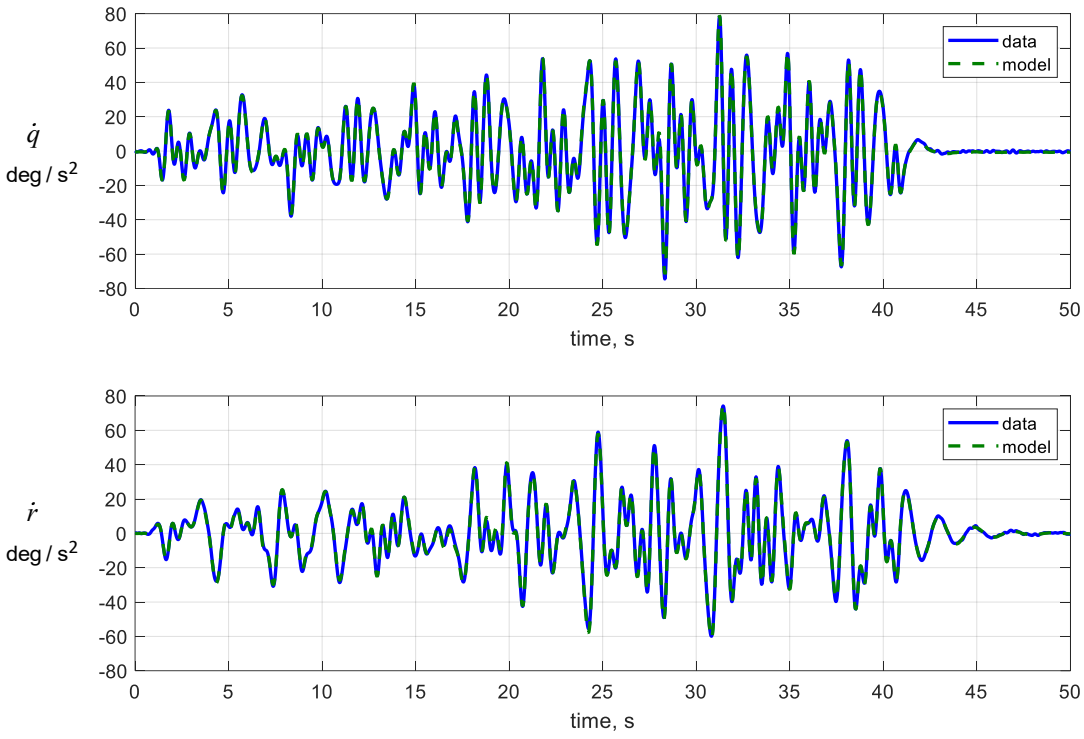

***Figure 6*. Model fit to angular acceleration data for a piloted F-16 large-amplitude maneuver with PTIs active**

V. E1 Subscale Aircraft Flight Test

The same approach described earlier and applied in the F-16 nonlinear simulation example was also applied to E1 subscale aircraft flight test data to estimate inertia parameters. Descending figure-eight maneuvers were flown at idle power by a pilot on the ground using conventional radio control, while automated orthogonal optimized multisine inputs (PTIs) were applied continuously to the elevator, rudder, and individual left and right ailerons. Rapid 360-degree velocity-vector rolls were executed on the straight legs of each descending figure-eight maneuver. The maneuvers were flown at idle power to minimize the gyroscopic effects from the angular momentum of the propulsion system.

Because the E1 flight test maneuvers were flown by a remote pilot on the ground, the pilot had no direct information on the nominal angle of attack. This led to high values of nominal angle of attack and sideslip angle during the rapid 360-degree velocity-vector rolls, with consequent nonlinear and unsteady aerodynamic effects. To enforce the requirement for linear aerodynamics, the velocity-vector roll data were omitted from the analysis, leaving only the data from the descending turns. In addition, only data points with angle of attack less than 7 deg were included in the analysis. These decisions were made based on model structure determination techniques applied to the flight data [1]. The aerodynamic model required only linear terms, based on statistical modeling metrics used for model structure determination, for data at angle of attack below 7 deg. Because this data selection process resulted in discarding some data from each maneuver, and to improve the results, data from the descending turn portions of five descending figure-eight maneuvers were combined for the equation-error analysis by simply stacking the selected data from each maneuver. Data smoothing was applied to the explanatory variable time series prior to the data point selection and data stacking. This was done to obtain accurate and unbiased parameter estimates in the equation-error formulation [1,32]. The PTIs shown in Figs. 1 and 2 were applied continuously throughout all of the five maneuvers. Figure 7 shows the E1 flight trajectory for one of the five descending turn maneuvers with PTIs active throughout the maneuver.

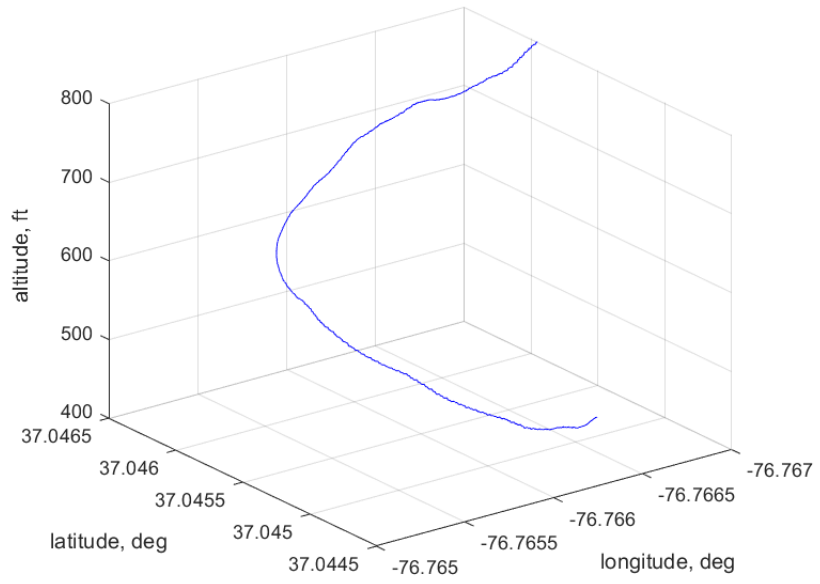

Figure 7. **E1 large-amplitude maneuver trajectory with PTIs active**

Figure 8 shows the E1 flight test data used for the equation-error parameter estimation, after removing the rapid velocity-vector roll data and prior to the data selection based on angle of attack. The flight data shown are concatenated data from five descending turn maneuvers, for a total of approximately 70 seconds of flight data.

The model fits to E1 flight data for angular acceleration in pitch and yaw are shown in Fig. 9. Coefficient of determination R^2 was 94.7% and 94.9% for the pitch and yaw angular accelerations, respectively. Table 3 shows the inertia parameters estimated from E1 flight test data, along with values obtained from ground testing using the same E1 aircraft. In this case, the inertia tensor elements were estimated directly, but still using the same equation-error formulation. As discussed earlier, this requires a nonlinear optimizer to obtain the inertia tensor parameter estimates, because the inertia tensor elements appear nonlinearly in the equations. SIDPAC program oe.m was used for this purpose.

The ground test values in Table 3 were determined using a tri-filar torsional pendulum for I_z and I_{xz}, an overhead pivot pendulum for I_x and I_y, a point-mass correction for a minor elevator repair, and corrections for air resistance based on measurements from similarly configured airframes. Uncertainty in the ground test results was estimated at less than ±3%.

The mean absolute difference in the flight test estimates relative to the ground-test results was less than 4%, with a maximum absolute percent difference of 5.80%, as shown in the last column of Table 3. Standard errors for the flight test results were computed using SIDPAC program m_colores.m to correct the equation-error model parameter uncertainties for colored residuals when the model parameterization is nonlinear, as is the case when estimating inertia tensor elements in the equation-error formulation. The results in Table 3 show that all ground-test values of the inertia parameters were within ±2 standard errors of the values estimated from E1 flight data, indicating that the flight estimates were in statistical agreement with the ground-test values.

The E1 flight test results demonstrate that the proposed approach is a feasible and accurate method for estimating moment of inertia parameters directly from flight test data.

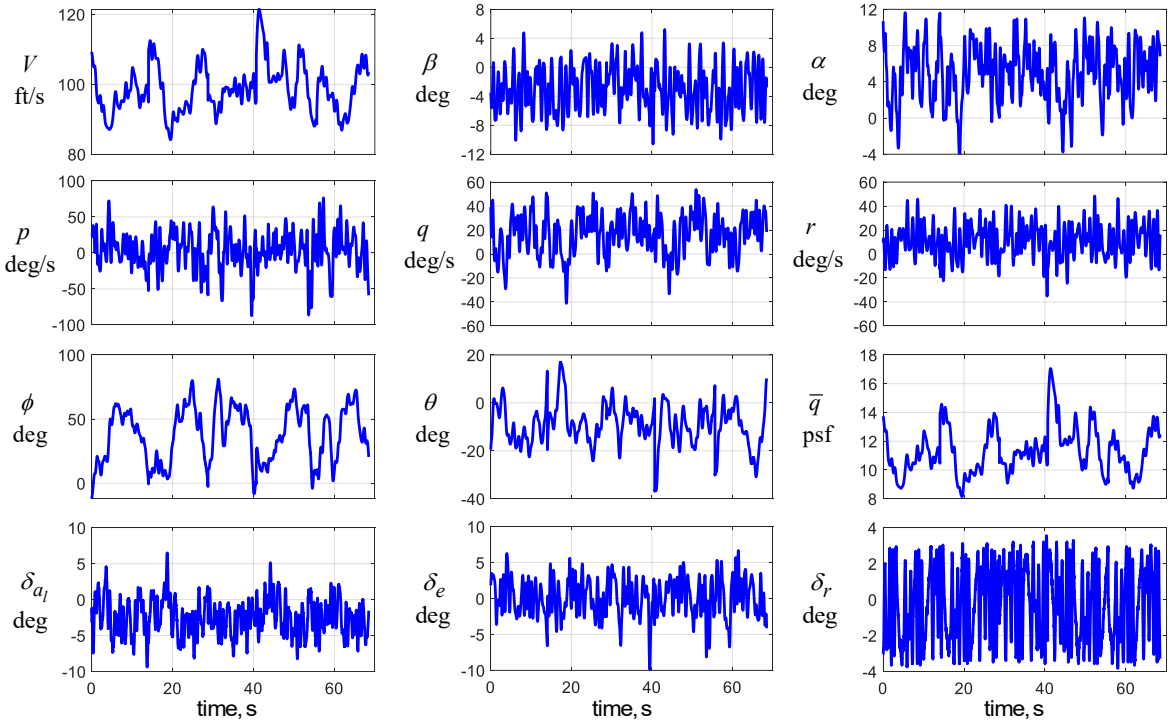

***Figure 8*. E1 large-amplitude maneuver data with PTIs active**

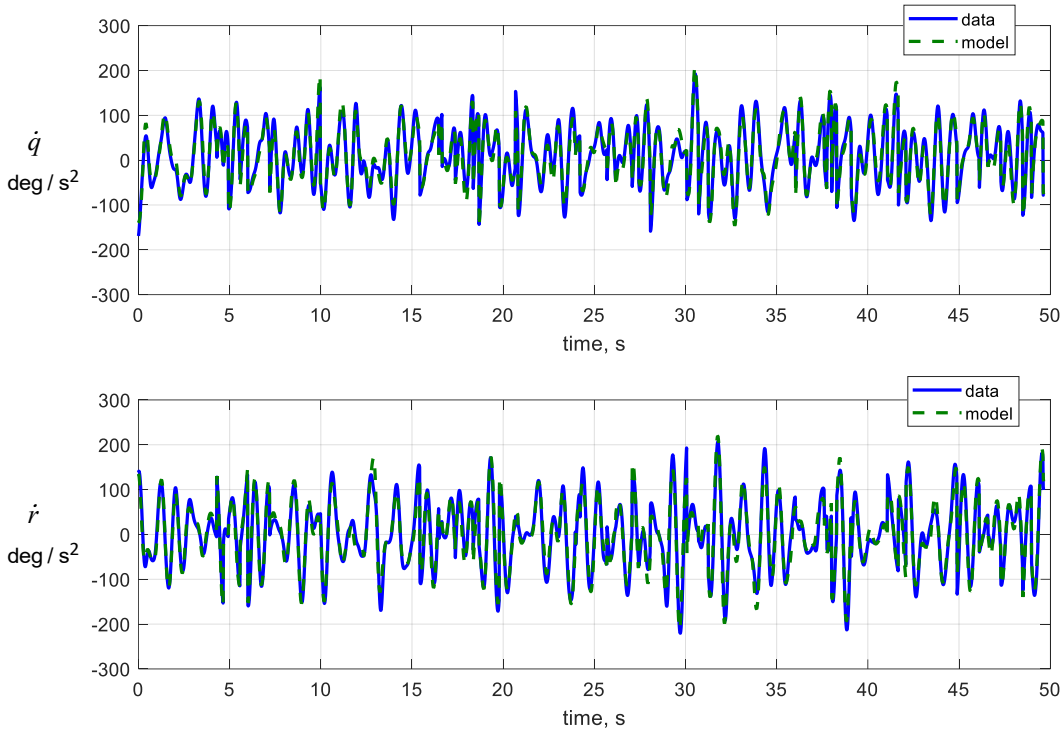

***Figure 9*. Model fit to angular acceleration data for piloted E1 large-amplitude maneuvers with PTIs active**

***Table 3*. E1 Inertia Parameters**

Parameter	Ground Test Estimate	Flight Test Estimate ± Standard Error	Percent Difference
I_x	2.964	3.053 ± 1.002	3.01
I_y	8.776	8.711 ± 0.732	–0.74
I_z	11.716	11.036 ± 0.475	–5.80
I_{xz}	0.750	0.779 ± 0.107	3.89

VI. Discussion

The F-16 nonlinear simulation and E1 flight test examples demonstrated that inertia parameters can be determined accurately using either linear estimation for $c_3, c_4, c_5,$ and c_6, or nonlinear estimation for $I_x, I_y, I_z,$ and I_{xz}. The latter approach is more direct, in that the results are the inertia tensor elements, and the calculated uncertainties apply directly to those quantities. However, it was found that the nonlinear estimation approach required more flight data to obtain good accuracy. The equation-error formulation accommodates this requirement, because it is easy to stack data from several maneuvers for one analysis, as was done for the five maneuvers flown on the E1 aircraft. The linear estimation approach requires less flight data, as demonstrated by the F-16 nonlinear simulation example, which used data from a single simulated flight test maneuver. This approach can also be implemented using real-time parameter estimation methods. The results are estimates of the inertia constants $c_3, c_4, c_5,$ and c_6 and associated uncertainties, which must then be converted to inertia tensor elements $I_x, I_y, I_z,$ and I_{xz} for nondimensional aerodynamic modeling. An analytic expression for the transformation from $c_3, c_4, c_5,$ and c_6 to $I_x, I_y, I_z,$ and I_{xz} [i.e., the inverse of Eq. (13)] could not be found, even with the assistance of symbolic mathematics software. However, it was found that a numerical nonlinear solver could be applied to find an accurate solution for the inverse transformation of Eq. (13).

It is likely that a variety of different large-amplitude maneuvers could be used successfully with the proposed method, which might result in even more accurate flight test results. A good maneuver for this problem will produce uncorrelated aerodynamic explanatory variable data at low nominal angles of attack and high angular rates. Given the capability to select data points from individual maneuvers and combine data from several maneuvers, the recommended approach is to fly multiple maneuvers to collect the required flight data, then select the data from those maneuvers that satisfy the requirements of low nominal angle of attack, low correlations among the aerodynamic explanatory variables, and high angular rates.

VII. Conclusions

A novel method for accurately estimating aircraft moments of inertia directly from flight test data was explained and demonstrated. The approach uses flight test data from maneuvers designed for high angular rates to make the nonlinear inertia terms significant, with simultaneous orthogonal optimized multisine excitations and low nominal

angle of attack for accurate linear aerodynamic parameter estimates. The required equations of motion and modeling techniques were developed and the method was demonstrated using simulated flight data from an F-16 nonlinear simulation. The method was then applied to flight test data from the E1 subscale aircraft, and the flight-estimated moments of inertia were compared with values obtained from ground testing using the same aircraft.

Results showed that the approach is feasible and accurate, but requires an instrumented aircraft that can be flown in maneuvers with high angular rates and an automated onboard excitation system. These requirements can be fulfilled by many subscale aircraft used in research and development, or by rapid-prototype aircraft. Previous flight tests have demonstrated that a skilled test pilot can implement effective multi-axis excitations with low correlations during large-amplitude maneuvers, so that it should be possible to use this technique without an onboard automated excitation system. Repeated maneuvers can be flown for improved accuracy and confidence in the results. The equation-error formulation can easily include or exclude data points from multiple maneuvers to satisfy the requirements of low nominal angle of attack with high angular rates. Applying data smoothing to the explanatory variable time series data prior to the data point selection produces parameter estimates that are unbiased and accurate. Results showed that errors in the aircraft moment of inertia parameters determined from simulated F-16 flight test maneuver data were less than 6% compared to the true values in the simulation. Flight test results for the E1 subscale aircraft were within 6% of ground-test values obtained using the same aircraft.

A good practical flight test procedure would be to first apply the proposed method to accurately estimate the inertia tensor elements, then proceed with stability and control flight testing using nondimensional aerodynamic modeling. The proposed flight test technique is faster than ground-based inertia testing, and the results shown in this work demonstrate that the accuracy is comparable. Risk to the airframe is arguably lower with the proposed flight test method, because fairly simple flight test maneuvers are required, whereas ground-based inertia testing typically involves swinging or oscillating the suspended aircraft in some way, or mounting the aircraft on an apparatus with springs and pivots. Furthermore, the statistical uncertainty associated with results of the flight test method can be computed accurately with well-established methods, whereas determining the uncertainty in results from ground-based inertia testing is more complex and difficult, because many error sources are involved.

The flight test method could be particularly useful for rapid-prototype aircraft, for efficient stability and control flight testing, or in situations where the aircraft design or configuration are changed often, or as a cross-check for ground-test or CAD results. The capability to accurately estimate moments of inertia from flight test data can speed

up aircraft development and decrease cost and risk by eliminating the need for ground testing or CAD modeling to obtain accurate moments of inertia. Because the method can be implemented in real time, other possible applications include real-time moment of inertia estimates for stores separation or changing fuel or loading conditions.

Acknowledgments

This research in aircraft system identification was funded by the NASA Transformational Tools and Technologies (TTT) project. The efforts of the E1 flight test team at NASA Langley in building and testing the aircraft and associated systems, carefully calibrating the instrumentation, and carrying out the flight operations to collect the high-quality flight test data used in this study are gratefully acknowledged. Dan Murri was the research pilot who skillfully flew the flight test maneuvers on the E1 aircraft. Ron Busan did the detailed ground testing and calculations to generate the ground-test values of the E1 moments of inertia used for comparison with flight test results.

References

[1] Morelli, E.A. and Klein, V., *Aircraft System Identification – Theory and Practice*, 2nd Edition, Sunflyte Enterprises, Williamsburg, VA, 2016, Chapters 3,5,6,8, and 11, and Appendices C and D.

[2] Dantsker, O.D., Vahora, M., Imtiaz, S., and Caccamo, M., "High Fidelity Moment of Inertia Testing of Unmanned Aircraft," *AIAA Applied Aerodynamics Conference*, AIAA Paper 2018-4219, June 2018. https://doi.org/10.2514/6.2018-4219

[3] Lorenzetti, J.S., Bañuelos, L.C., Clarke, R., Murillo, O.J., and Bowers, A.H., "Determining Products of Inertia for Small Scale UAVs," *2017 AIAA SciTech Forum*, AIAA Paper 2017-0547, January 2017. https://doi.org/10.2514/6.2017-0547

[4] Lehmkühler, K., Wong, K.C., and Verstraete, D., "Methods for Accurate Measurements of Small Fixed Wind UAV Inertial Properties," *The Aeronautical Journal*, Vol. 120, No. 1233, 2016, pp. 1785-1811. https://doi.org/10.1017/aer.2016.105

[5] Chin, A.W., Herrera, C.Y., Spivey, N.D., Fladung, W.A., and Cloutier, D., "Experimental Validation of the Dynamic Inertia Measurement Method to find the Mass Properties of an Iron Bird Test Article," *2015 AIAA SciTech Forum*, AIAA Paper 2015-2060, January 2015. https://doi.org/10.2514/6.2015-2060

[6] Previati, G., Gobbi, M., and Mastinu, G., "Method for the Measurement of the Inertia Properties of Bodies with Aerofoils," *Journal of Aircraft*, Vol. 49, No. 2, 2012, pp. 444-452. https://doi.org/10.2514/1.C031369

[7] Jardin, M.R. and Mueller, E.R., "Optimized Measurements of Unmanned-Air-Vehicle Mass Moment of Inertia with a Bifilar Pendulum," *Journal of Aircraft*, Vol. 46, No. 3, 2009, pp. 763-775. https://doi.org/10.2514/1.34015

[8] Peterson, W.L., "Mass Properties Measurement in the X-38 Project," *63rd Annual Conference of the Society of Allied Weight Engineers, Inc.*, SAWE Paper 3325, Category 6, May 2004.

[9] de Jong, R.C. and Mulder, J.A., "Accurate Estimation of Aircraft Inertia Characteristics from a Single Suspension Experiment," *Journal of Aircraft*, Vol. 24, No. 6, 1987, pp. 362-370. https://doi.org/10.2514/3.45454

[10] Wolowicz, C.H. and Yancy, R.B., "Experimental Determination of Airplane Mass and Inertial Characteristics," NASA TR R-433, 1974.

[11] Perry, D.H., "Measurements of the Moments of Inertia of the Avro 707B Aircraft," C.P. No. 647, Ministry of Aviation, London, UK, 1963.

[12] Wener, N.L., "Measurement of Aircraft Moments of Inertia," AGARD Report 248, 1959.

[13] Turner, H.L., "Measurement of the Moments of Inertia of an Airplane by a Simplified Method," NACA TN 2201, 1950.

[14] Gracey, W., "Experimental Determination of the Moments of Inertia of Airplanes by a Simplified Compound-Pendulum Method," NACA TN 1629, 1948.

[15] Soulé, H.A. and Miller, M.P., "The Experimental Determination of the Moments of Inertia of Airplanes," NACA Report 467, 1933.

[16] Miller, M.P. "An Accurate Method of Measuring the Moments of Inertia of Airplanes," NACA TN 351, 1930.

[17] Green, M.W. "Measurement of the Moments of Inertia of Full Scale Airplanes," NACA TN 265, 1927.

[18] Mutluay, T., "The Development of an Inertia Estimation Method to Support Handling Quality Assessment," Master of Science Thesis, Delft University of Technology, Delft, The Netherlands, September 2015.

[19] Parikh, K.K., Dogan, A., Subbarao, K., Reyes, A., and Huff, B., "CAE Tools for Modeling Inertia and Aerodynamic Properties of an R/C Airplane," *AIAA Atmospheric Flight Mechanics Conference*, AIAA Paper 2009-6043, August 2009. https://doi.org/10.2514/6.2009-6043

[20] Jordan, T.L., Langford, W.M., and Hill, J.S.; "Airborne Subscale Transport Aircraft Research Testbed: Aircraft Model Development", *AIAA Guidance, Navigation, and Control Conference and Exhibit*, AIAA Paper 2005-6432, August 2005. https://doi.org/10.2514/6.2005-6432

[21] Pegram, J.P. and Anemaat, W.A., "Preliminary Estimation of Airplane Moments of Inertia using CAD Solid Modeling," *General Aviation Technology Conference and Exposition*, SAE Paper 2000-01-1700, May 2000. https://doi.org/10.4271/2000-01-1700

[22] Muliadi, J., Langit, R., and Kusumoputro, B., "Estimating the UAV moments of inertia directly from its flight data," *2017 15th International Conference on Quality in Research (QiR) : International Symposium on Electrical and Computer Engineering*, IEEE, New York, NY, July 2017, pp. 190-196. https://doi.org/10.1109/QIR.2017.8168480

[23] Alsharif, M.A. and Hölzel, M.S., "Estimation of a drone's rotational dynamics with piloted Android flight data," *2016 IEEE 55th Conference on Decision and Control (CDC)*, IEEE, New York, NY, December 2016, pp. 1199-1204. https://doi.org/10.1109/CDC.2016.7798429

[24] Nainer, C., Garnier, H., Gilson, M., and Pittet, C., "In-Orbit Data Driven Identification of Satellite Inertia Matrix," *IFAC PapersOnLine*, Vol. 51, Issue 15, 2018, pp. 467-472.
https://doi.org/10.1016/j.ifacol.2018.09.189

[25] Keim, J.A., Acikmese, A.B., and Shields, J.F., "Spacecraft Inertia Estimation via Constrained Least Squares," *2006 IEEE Aerospace Conference*, IEEE AC Paper No. 1487, March 2006.
https://doi.org/10.1109/AERO.2006.1655995

[26] Psiaki, M.L., "Estimation of a Spacecraft's Attitude Dynamics Parameters by Using Flight Data," *Journal of Guidance, Control, and Dynamics*, Vol. 28, No. 4, 2005, pp. 594-603.
https://doi.org/10.2514/1.7362

[27] Wilson, E., Lages, C., and Mah, R., "On-line gyro-based, mass-property identification for thruster-controlled spacecraft using recursive least squares," *The 2002 45th Midwest Symposium on Circuits and Systems, MWSCAS-2002*, IEEE, New York, NY, September 2002, pp. II-334-II-337.
https://doi.org/10.1109/MWSCAS.2002.1186866

[28] "System IDentification Programs for AirCraft (SIDPAC)," NASA Technology Transfer Program, https://software.nasa.gov/software/LAR-16100-1 [retrieved 21 July 2021].

[29] "SIDPAC Software," http://sunflyte.com/SIDBook_SIDPAC.htm#SIDPAC_Users [retrieved 21 July 2021].

[30] Morelli, E.A. and Grauer, J.A. "Practical Aspects of Frequency-Domain Approaches for Aircraft System Identification," *Journal of Aircraft*, Vol. 57, No. 2, March 2020.
https://doi.org/10.2514/1.C035599

[31] Press, W.H., S.A. Teukolsky, W.T. Vettering, and B.R. Flannery *Numerical Recipes in FORTRAN: The Art of Scientific Computing*, 2nd Edition, Cambridge University Press, New York, NY, 1992, Chapter 10.

[32] Morelli, E.A., "Practical Aspects of the Equation-Error Method for Aircraft Parameter Estimation," *AIAA Atmospheric Flight Mechanics Conference*, AIAA Paper 2006-6144, August 2006.
https://doi.org/10.2514/6.2006-6144

[33] Durham, W.C., Lutze, F.H., and Mason, W., "Kinematics and Aerodynamics of Velocity-Vector Roll," *Journal of Guidance, Control, and Dynamics*, Vol. 17, No. 6, 1994, pp. 1228-1233.
https://doi.org/10.2514/3.21337

[34] Morelli, E.A. "Multiple Input Design for Real-Time Parameter Estimation in the Frequency Domain," *13th IFAC Symposium on System Identification*, Paper REG-360, August 2003.
https://doi.org/10.1016/S1474-6670(17)34833-4

[35] Morelli, E.A. "Flight-Test Experiment Design for Characterizing Stability and Control of Hypersonic Vehicles," *Journal of Guidance, Control, and Dynamics*, Vol. 32, No. 3, May-June 2009, pp. 949-959.
https://doi.org/10.2514/1.37092

[36] Morelli, E.A. "Flight Test Maneuvers for Efficient Aerodynamic Modeling," *Journal of Aircraft*, Vol. 49, No. 6, November-December 2012, pp. 1857-1867.
https://doi.org/10.2514/1.C031699

[37] Morelli, E.A. "Practical Aspects of Real-Time Modeling for the Learn-To-Fly Concept," *AIAA Atmospheric Flight Mechanics Conference*, AIAA Paper 2018-3309, June 2018.
https://doi.org/10.2514/6.2018-3309

[38] Brandon, J.M. and Morelli, E.A. "Real-Time Global Nonlinear Aerodynamic Modeling from Flight Data," *Journal of Aircraft*, Vol. 53, No. 5, September-October 2016, pp. 1261-1297.
https://doi.org/10.2514/1.C033133

[39] Riddick, S.E., Busan, R.C., Cox, D.E., and Laughter, S.A., "Learn-to-Fly Test Setup and Concept of Operations," *AIAA Atmospheric Flight Mechanics Conference*, AIAA Paper 2018-3308, June 2018.
https://doi.org/10.2514/6.2018-3308

[40] Riddick, S.E., "An Overview of NASA's Learn-to-Fly Technology Development," *2020 AIAA SciTech Forum*, AIAA Paper 2020-0760, January 2020.
https://doi.org/10.2514/6.2020-0760